Journal of
Marine Science and Engineering

MDPI

Article

Experimental Study of Submarine Pipeline with Geotextile and Stone Cover Protection Under the Superposition of Waves and Currents

Wenqi Si [1], Mingqing Wang [2], Yaru Gao [3], Ke Sun [1,*], Bing Chen [1], Risheng Wang [1], Lin Cui [2], Dong-Sheng Jeng [2,4] and Hongyi Zhao [2]

1 College of Transportation and Civil Engineering, Shandong Jiaotong University, Jinan 250357, China; 19861836034@163.com (W.S.); chenbing142857@tju.edu.cn (B.C.); 204055@sdjtu.edu.cn (R.W.)
2 College of Civil Engineering, Qingdao University of Technology, Qingdao 266033, China; wmqing2000@163.com (M.W.); cuilin@qut.edu.cn (L.C.); d.jeng@griffith.edu.au (D.-S.J.); hyzhaohhu@gmail.com (H.Z.)
3 College of Harbor, Coastal and Offshore Engineering, Hohai University, Nanjing 210098, China; yaru6998@163.com
4 School of Engineering and Built Environment, Griffith University, Gold Coast Campus, Southport, QLD 4222, Australia
* Correspondence: 210114@sdjtu.edu.cn

Abstract: Submarine pipelines are the main transport carriers of marine resources. In order to protect these pipelines, geotextile and stone covering measures are adopted in this paper and the protective effect is studied. A sequence of physical model tests was conducted to carry out the research. The hydrodynamic characteristics and seabed oscillation response of the seabed surrounding the pipeline were analyzed with or without geotextile and stone cover protection, and it was found that they were affected by waves (and currents). The experimental results show the following: (1) comparing the regular wave and current with the regular wave alone, it is found that forward current promotes wave propagation and reverse current inhibits wave propagation; (2) the protective effect of geotextile and stone covering measures on different positions of the pipeline (the front, the bottom, and the back of the pipe) is basically same; (3) in the case of waves with large wave heights and long wave periods superimposed with ocean currents, the protective effect of geotextile and stone coverings on the hydrodynamic and seabed pore pressure around the pipeline is more significant.

Keywords: submarine pipeline protection; geotextile and stone cover protection; oscillatory pore pressure; hydrodynamics; wave flume experiment

Citation: Si, W.; Wang, M.; Gao, Y.; Sun, K.; Chen, B.; Wang, R.; Cui, L.; Jeng, D.-S.; Zhao, H. Experimental Study of Submarine Pipeline with Geotextile and Stone Cover Protection Under the Superposition of Waves and Currents. *J. Mar. Sci. Eng.* **2024**, *12*, 2218. https://doi.org/10.3390/jmse12122218

Academic Editor: Abdellatif Ouahsine

Received: 12 November 2024
Revised: 25 November 2024
Accepted: 28 November 2024
Published: 3 December 2024

1. Introduction

With the continuous development and advancement of marine engineering, submarine pipelines play a crucial role in the transportation of oil and gas resources across oceans. These pipelines are lifelines deep beneath the sea, consistently delivering precious marine resources to various parts of the world, meeting the enormous demand for energy. However, at the same time, damage and failure incidents of submarine pipelines occur from time to time. These incidents not only pose potential threats to the marine environment, but could also disrupt the normal transportation of marine resources, potentially leading to significant safety accidents [1,2]. Therefore, the stability of pipelines has become a global hotspot among both coastal and geotechnical engineers [3]. Research results show that seabed deformation due to wave (current) action, seabed liquefaction [4–7], and accidents caused by fishing activities or falling objects [8,9] are among the major factors in the failure of submarine pipelines. It is widely recognized that an increase in pore pressure will lead to a decrease in effective stress, which directly leads to the weakening of soil strength and the enhancement of compressibility. Under the action of waves and currents, these changes can significantly affect the stability of the ocean's structure. Therefore, it is critically important to delve into the dynamic response of the seabed surrounding submarine pipelines under the influence of waves (and currents), as well as to develop protection strategies for submarine pipelines and the surrounding seafloor.

The effect of the liquefaction potential of seafloor soil on the instability of marine structures cannot be ignored. The dynamic wave pressure generated by the wave and current load is applied to the seafloor surface, resulting in significant changes in the size and distribution of pore water pressure and effective stress inside the seabed. The soil at the bottom of the sea is in a saturated condition (above the water table), and at a point, in the interior of the soil, the effective stress conditions may instantly change or even be cancelled out by an increase in pore water pressure ($u_0 + \Delta u$) due to an external and instantaneous stress (u_0 is the initial effective stress). When the upward component of pore pressure is greater than the gravity of soil particles, the soil particles are in a suspended state, resulting in soil liquefaction, and then the seabed surface loses all bearing strength, resulting in structural instability. Therefore, in order to better protect the pipeline from the impact of soil instability, the pipeline can be buried at a certain depth. Sudhan et al. [10] conducted a simulation study on a pipeline buried under the seabed, examining the mechanism of pore water pressure surrounding the pipeline under different wave conditions and burial depth ratios. Zhou et al. [11] modeled pipelines in three semi-buried or resting soils considering the isotropic action of regular waves, and found that the superposition of water flow in the same direction of the waves increased pore pressure and thus increased the probability of seafloor liquefaction. Based on the study of codirectional regular wave flow, Chen et al. [12] extensively examined the impact of wave flow inversion on pore pressure around pipelines in trenches and seabed liquefaction. The experimental results revealed that when the direction of the current aligns with the wave propagation, the risk of liquefaction around the pipe significantly increases; conversely, if the current direction opposes the wave propagation, this helps to reduce the likelihood of soil liquefaction. Zhai et al. [13] conducted a series of regular wave tests and numerical modeling analyses, adding variables such as sand grain size and pipeline diameter on the basis of varying different backfill depths. However, only the wave-induced pore pressures within the circular area around the buried sandy seabed pipeline were analyzed, which has certain limitations. Sun et al. [14] not only demonstrated the pore pressure values on the surface of a partially buried pipeline through flume tests, but also systematically evaluated the variations in pore pressure within the gully sediment stratum surrounding the pipeline and its immediate vicinity. The findings indicated that a deeper gully depth and a thicker buried stratum can significantly reduce the pore water pressure across the entire trench zone, meaning that the greater the burial depth of the pipeline, the less it is affected by seabed instability; thereby, enhanced shelter can be used as a measure to protect submarine pipelines from the effects of transient seafloor liquefaction. On the other hand, Gao et al. [15] explored pore pressure variations due to waves in the pulverized bed around buried pipelines and partially/fully backfilled pipelines. The measured data not only confirm that residual pore pressure is the primary cause of liquefaction in pulverized soil, but also demonstrate that full backfilling, as an economically effective protective method, significantly reduces liquefaction risks and ensures the safety and stability of pipelines in pulverized seabed. This conclusion further enhances the significance of adapting the construction of marine infrastructure in different soil circumstances.

In addition to adjusting the buried depth of the pipeline, the use of the rock berm protection method can also be considered [16]. Sekiguchi et al. [17] conducted four experiments (two test plots had gravel covering the entire soil surface, and the remaining two test plots had gravel only covering part of the soil surface) to explore the effects of varying the thickness and width of gravel cover on fine sand sediments. The experimental results indicate that using gravel/stone block/riprap covering may be an effective measure to protect soil (whether hydraulically filled or naturally deposited) from liquefaction. Subsequently, Sumer et al. [18] carried out an experimental study on stone covering (including the influence of the intermediate filter layer) on the silt seabed under the action of continuous waves and analyzed in depth the effects of stone accumulation density and the number of stone layers on the distribution depth of pore pressure across the entire soil layer. As the experimental data indicate, under the action of continuous waves, the presence of covered stone decreases the liquefaction potential, which is mainly related to the density of stone accumulation and the quantity of stone layers. Moreover, the sinking displacement of stone in soil can be effectively reduced by increasing the filter layer. The studies above are all focused on covering the seabed surface with stone layers, and do not consider the existence of structures such as pipelines. Later, Sumer et al. [19] studied the stability of rock berm (three different berm materials were used, respectively) laid above a pipeline in a trench under the action of large waves and obtained a critical mobility number corresponding to the initial movement of the rock berm, according to the experimental results. In addition to covering the upper part of the pipeline with a stone safeguarding layer, Tauqeer and Yin et al. [20,21] calculated the load carrying capacity and discussed the geometric optimization of three shapes of GRP protective covers via the finite element method (FEM), with the aim of addressing the problem of submarine pipelines subjected to the load of fishing activities and the impact of falling objects. This laid a foundation for the selection and use of a GRP shield (a subsea protection cover designed by PJNC company to protect offshore oil and gas pipelines from falling objects, manufactured from concreate as well as Glass-Reinforced Plastic ("GRP"); it is low cost, lightweight, and easy to install). The above pipeline protection measures are based on the concept of covering pipelines with rigid protective layers to withstand the influence of ocean currents and heavy load impacts. In addition, covering them with flexible protective pads is also an effective protection method. Geotextiles are engineering synthetic materials widely used in marine and civil engineering. They can prevent fine soil particles from passing through while allowing water and other fluids to flow smoothly, which is crucial for preventing soil erosion and protecting infrastructure. Therefore, geotextiles can be used as protective layers to prevent waves or other biological damage to marine infrastructure. Additionally, this structure can resist chemical corrosion (this experiment utilizes this property of geotextiles). Furthermore, the reinforcing effect of geotextiles gives them a certain tensile strength, enhancing the overall strength and stability of the soil, especially in weak foundations or areas that need reinforcement [22–24]. Aside from covering pipelines with protective layers, there are also structural support measures (specifically including grout bag support, underwater pile support, and riprap support) to prevent pipe instability and failure due to overhanging spans caused by topography. Xie et al. [25] and Zhang et al. [26] have conducted comprehensive reviews and detailed analyses of the experimental research and progress in the field of pipeline protection.

The aforementioned research on protective pipeline coverings mainly focuses on the stability of the protective measures. Only a few studies focus on the mechanisms of changes in hydrodynamic motion around submarine pipelines and submarine response under the action of protective measures. Hence, a comprehensive set of scale model pipeline tests are performed in this study in a wave flume to investigate both wave dynamics and seabed reactions in the vicinity of pipelines, considering scenarios with and without the application of geotextiles and stone cover protection. The protective effect of the measures, i.e., the geotextiles and stones, on pore pressure is comprehensively examined under various wave and current conditions. To the best of the author's knowledge, this is the first experimental study of wave-current-induced pore pressure around geotextile and stone coverings that protect pipelines. In Section 2, the experimental arrangements and workflow are thoroughly described. Section 3 examines and analyzes both the hydrodynamic characteristics of the flow fields and the spatial distribution of seafloor pore pressure around the protective pipeline. Eventually, the crucial discoveries of this paper are concluded in Section 4.

2. Wave Flume Experiments

Investigating the hydrodynamic features and seabed responses in the area around undersea pipelines affected by wave (and current) interactions is of significant importance. To this end, physical model experiments on waves and pipelines were conducted in the wave flume at the Harbor and Waterway Hydrodynamic Laboratory of Shandong Jiaotong University, simultaneously recording variations in wave contour, dynamic wave pressure, and pore pressure around the pipeline and its seabed. Specifically, the impact of geotextile and stone cover protection measures on the hydrodynamic performance and seabed response in the proximity of the undersea pipeline was assessed, with a focus on the protective advantages compared to a bare pipeline.

2.1. Experimental Setup

The wave generation facility required for this experiment not only has the capability to generate regular waves, but also random waves, as well as unidirectional and reciprocating currents. The detailed design and layout are depicted in Figure 1. An electrically driven hydraulic piston wave generator is installed upstream in the wave tank, and a wave absorber is installed downstream to consume incident wave energy, thereby minimizing wave reflection effects on the experiment. By manually adjusting the frequency inverter, a bidirectional fluid field with waves in the same direction or reverse direction can be created, enabling the simulation of a uniform fluid field in flume experiments. This study considers three scenarios: regular waves alone, regular waves combined with forward flow, and regular waves combined with reverse flow. The wave generator is designed to produce waves with heights ranging from 0 to 0.25 m, wave periods from 1.0 to 4.0 s, and water depths from 0.1 to 1.0 m. Throughout this series of physical simulation experiments, the water depth consistently remains at 0.45 m, where the velocity of the reversible steady flow can reach up to approximately 0.3 m per second.

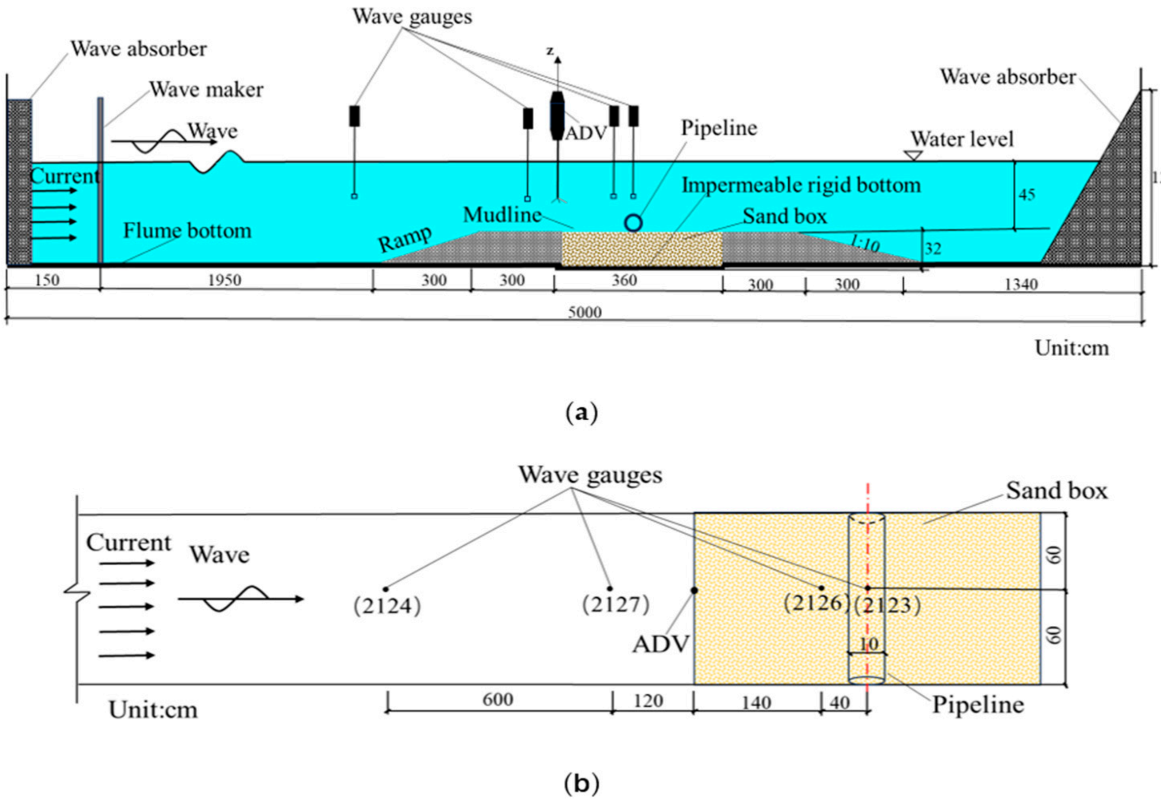

Figure 1. Experimental equipment: (**a**) wave trough; (**b**) location of the wave sensors.

During the setup and data acquisition process of the physical experiments, one acoustic Doppler velocimeter (ADV) designed by Nortek AS in Norway, four wave-height gauges (WHG2123, WHG2124, WHG2126, and WHG2127—refer to Figure 1b), eight wave-pressure transducers, and fifteen pore-pressure transducers (Figure 2) were employed to simultaneously collect and statistically analyze the flow velocities, wave profiles, wave pressures, and pore pressures around the pipe and seabed. The ADV was positioned 2.3 m from the center of the pipe and 0.3 m above the seabed surface, measuring the undisturbed flow velocity. The four wave-height gauges, designed by Nanjing Intelligent Technology Co., Ltd. in Nanjing, China (YWH203-D, with a range of 0 to 0.60 m and a precision of ±0.15%), were utilized to observe real-time variations in the free surface altitude.

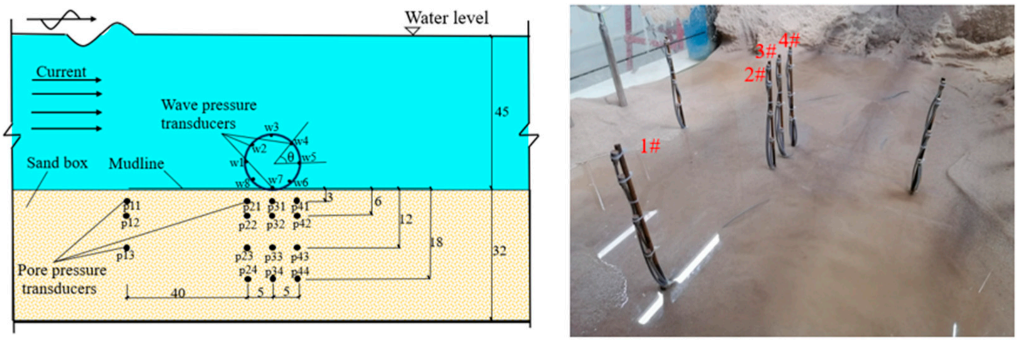

(**a**) (**b**)

Figure 2. Locations of wave-pressure transducers and pore-pressure transducers: (**a**) sensor layout diagram; (**b**) experimental field diagram.

The flume test is based on the following criteria for Frude numbers (Fr):

$$\lambda_{Fr} = \frac{\lambda_{Um}}{\lambda_g^{\frac{1}{2}} \lambda_g^{\frac{1}{2}}} \tag{1}$$

where λ_g = 1, we can obtain the following:

$$\lambda_{Um} = \lambda_D{}^{\frac{1}{2}} \tag{2}$$

$$\lambda_T = \frac{\lambda_D}{\lambda_{Um}} = \lambda_D{}^{\frac{1}{2}} \tag{3}$$

$$\lambda_{KC} = \frac{\lambda_{Um}\lambda_T}{\lambda_D} = 1 \tag{4}$$

The above derivation shows that the flume test can satisfy the requirements for both the Fr and KC values. Moreover, the Fr values of the shore deposits in the South China Sea [27] range from 0 to 0.5, and the KC values range from 0 to 20, reflecting the range used in this laboratory experiment. The detailed dimensions chosen in this paper are referenced in Wang et al. [28].

2.2. Measuring Instrumentation

During the physical experiments, an acoustic Doppler velocimeter (ADV), four wave-height gauges (WHG2123, WHG2124, WHG2126, and WHG2127—refer to Figure 1b), eight wave-pressure transducers, and fifteen pore-pressure transducers (Figure 2) were utilized to simultaneously measure and statistically analyze the flow velocities, wave profiles, wave pressures, and pore pressures around the pipe and the seabed. The ADV was located 2.3 m from the center of the pipe and 0.3 m above the seabed surface, measuring the undisturbed flow velocity. The four wave-height gauges, designed by Nanjing Intelligent Technology Co., Ltd. in Nanjing, China (YWH203-D, with a range of 0 to 0.60 m and a precision of ±0.15%), were employed to monitor real-time changes in the free-surface elevation. Among these wave-height gauges (seen in Figure 1), a far-field gauge, notated as wave-height gauge 2124, was allocated 7.8 m away from the center of the pipe to record the incident wave characteristics. The remaining three wave gauges (WHG2123, WHG2124, WHG2126, WHG2127) were arranged 1.8 m in front of, above, and behind the center of the pipe to capture the wave property alterations surrounding the pipe and explore the evolution of the wave profiles passing by the porous seabed. Eight CY302 miniature intelligent pressure sensors and fifteen CY303 pore-water intelligent pressure sensors, are both engineered and produced by Chengdu Keda Sheng ying Co., Ltd. (Chengdu, China), were applied to measure wave pressure and pore water pressure, respectively. The outer diameters of these pressure sensors are 6 mm and 8 mm. Their measurement ranges are 0 to 20 kPa and 0 to 30 kPa, respectively, with a precision of ±0.1%. The arrangement details are shown in Figure 1. Eight pressure transducers were deployed at fixed intervals of $\pi/4$ surrounding the circumference of the pipe. Note that the wave piezometer probes were passed through the inside of the pipe and secured by wrapping with raw material bands, resulting in the sensor surfaces being on the same plane as the structure surface. Fifteen pore-pressure transducers were buried at various depths and positions within a sandy seabed, with numbering based on the wave propagation direction from left to right. The wave propagation direction from left to right was sequentially numbered 1 to 4 and the depth direction from the seabed surface to the bottom was also sequentially numbered 1 to 4, and the detailed numbering and layout of the sensors in the vicinity of the pipe are depicted in Figure 2. Additionally, signals from the wave gauges, ADV, wave pressure sensors, and pore pressure sensors were synchronously collected at a data acquisition frequency of 100 Hz via a remote computer linked to the servo and data acquisition systems (see Figure 3a). By comprehensively analyzing the obtained sample signals, the mechanism of interaction between the seabed and waves (currents) around the submarine pipe under protection measures was obtained.

(**a**) (**b**) (**c**)

Figure 3. Locations of wave-pressure transducers and pore-pressure transducers: (**a**) acquisition devices; (**b**) pipes and fixtures; (**c**) wave-pressure gauge layout.

2.3. Properties of Samples

A submarine pipe model was created using a polyvinyl chloride (PVC) pipe, which had an outer diameter (D) of 0.1 m and a 0.01-m wall thickness. This pipe was positioned perpendicular to the seafloor to minimize interactions between the flume walls and the pipes; the pipe length was set to 1.19 m in alignment with the wave propagation direction, slightly shorter than the wave tank's internal width (refer to Figure 3b). The experimental findings indicated that a narrow gap (0.01 m) between the pipeline and the flume wall has minimal impact on the water flow field, simplifying the simulation of the wave (and current)–seafloor–pipe interaction to a two-dimensional problem. Furthermore, a specialized steel frame securely restricts the pipe's movement, ensuring it remains stationary and cannot rotate during the experiment.

As for the layout of the protective geotextile and stone covering measures, the geotextile was cut into a rectangle with a length of 1.2 m and a width of 0.4 m (according to the scouring range of Xu Y et al.'s [29] pipe scouring test) and tightly fitted around the pipe. In order to protect the probe of the wave pressure sensor on the surface of the pipe from damage, flat pebbles with a diameter of 3–8 cm were first stacked. Then, the gaps were filled with black gravel with a diameter of 1.2–1.8 cm to ensure that the pipe was completely covered to the greatest extent, as shown in Figure 4. In actual circumstances, different specifications of waste stone can be used, making this a very economical and environmentally friendly method.

Figure 4. The geotextile- and stone-covered pipe protection measure.

The test employed non-cohesive sand with an average particle size of d_{50} = 0.2037 mm as the seabed material. Its main physical properties are detailed in Table 1. A major limitation of the wave flume experiment is the inability to replicate the full-scale stress conditions of an actual site; thus, the study did not adopt the scaling rules for seabed soils. During sampling, the dry density ρ_d and specific gravity G_s of the soil samples were determined using the cutting ring method and the volumetric flask method, respectively. Based on the proportional relationship between the permeability coefficient and hydraulic gradient, the permeability coefficient k_s of the sandy soil was obtained through constant head permeability tests. The elastic modulus E was measured using a triaxial apparatus. According to empirical values, the Poisson's ratio μ of the soil sample was assumed to be 0.30. Consequently, the shear modulus G was derived from the relation $G = E/2(1 + \mu)$. Prior to the test, the porosity of the sandy soil was measured using the density method, and the porosity ratio was calculated using the formula $e = n/(1 - n)$. The sand from the model was screened to determine the grain size grading curve (illustrated in Figure 5), where d_{10} symbolizes the effectual particle size, d_{50} is the median particle size, c_u (1.3553) is the non-uniformity coefficient, and c_c (0.9893) is the curvature coefficient. The permeability coefficient was determined through constant head permeability tests. Before the experiment, water was introduced into the tank and allowed to stand for three days, ensuring complete settling of the sea bottom, negligible changes in porosity, and near-complete saturation. The water level height for all tests remained at 0.45 m.

Table 1. Soil properties.

Parameters	Symbol	Value
Mean grain size	d_{50} (mm)	0.2037
Dry density	ρ_d (g/cm^3)	1.5337
Maximum dry density	ρ_{dmax} (g/cm^3)	1.6076
Minimum dry density	ρ_{dmin} (g/cm^3)	1.2963
Specific gravity	G_s (g/cm^3)	2.6540
Permeability coefficient	k_s (m/s)	7.67×10^{-4}
Shear modulus	G (MN/m^2)	9.23
Poisson's ratio	μ	0.30
Porosity	n	0.4221
Void ratio	e	0.7304
Relative density	D_r	0.7994

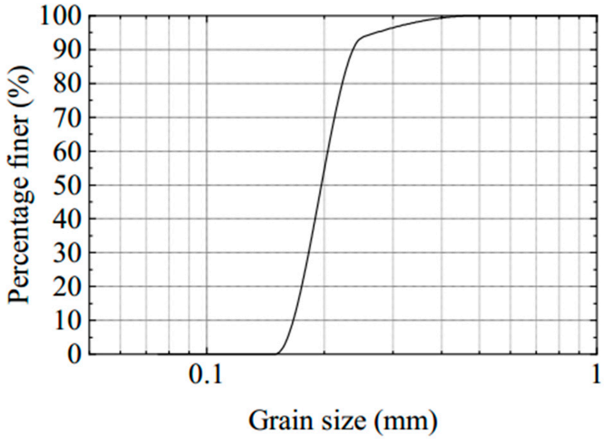

Figure 5. Distribution curve of model sand particle size: d_{50} = 0.2037 mm, d_{10} = 0.1564 mm, d_{30} = 0.1811 mm, d_{60} = 0.2119 mm, c_u = 1.3553, and c_c = 0.9893.

2.4. Experimental Conditions and Procedures

The experimental wave (and current) conditions are detailed in Table 2, including regular waves characterized by diverse wave parameters, which are either accompanied by forward or reverse currents. The wave height (H) is uniformly adjusted in increments of 0.02 m, ranging from 0.08 m to 0.14 m; the wave period (T) increases from 1.2 s to 1.8 s at intervals of 0.2 s. The current velocity (U) is set within the range of −0.2 m/s to 0.2 m/s, increasing in increments of 0.1 m/s. A positive or negative sign merely indicates the direction of water flow relative to the propagation of waves, with a positive sign indicating currents moving in the same direction as the waves and a negative sign indicating the presence of a reverse current. For all tests, the water depth (h) above the sediment basin was maintained at a constant 0.45 m. This study set up a total of 2 control groups: one group had geotextile- and stone-covered pipes, while the other group had unprotected exposed pipes placed on the seabed. The tests were conducted under 11 different wave–current conditions (as shown in Table 2). A total of 22 experimental tests were executed, and relevant data were collected and sorted. Each set of test data was collected three times to ensure precision, and the final processed findings are the averages of the data collected in the three tests.

Table 2. Test conditions.

Case No.	Wave Height H (m)	Wave Period T (s)	Current U (m/s)
1	0.08	1.6	-
2	0.10	1.6	-
3	0.12	1.6	-
4	0.14	1.6	-
5	0.10	1.2	-
6	0.10	1.4	-
7	0.10	1.8	-
8	0.10	1.6	0.1
9	0.10	1.6	0.2
10	0.10	1.6	−0.1
11	0.10	1.6	−0.2

The layout and test processes for specific model pipes and protective measures are as follows:

(1) Placement of facilities and instrumentation: Eight wave-pressure transducers were routed through the inside of the pipe, mounted in drilled holes around the pipe, and wrapped with raw tape to ensure that the instruments nested tightly into the

pipe and did not fall out. Fifteen additional pore-water-pressure transducers were affixed to specialized steel frames along the depth of the sediment bed at the base of the sedimentation basin, requiring placement prior to sand filling. Due to the presence of sand filters on the surface of these pore-pressure transducers, they must be completely immersed in water for a minimum duration of 24 h to guarantee the complete expulsion of air. Furthermore, along the central axis of the wave tank, four wave-height gauges and one ADV were set up. Next, the model pipe was placed and secured by support components to limit the movement of the model pipe. Finally, the geotextile covered the pipe, and then stones of different particle sizes were placed in turn, so that the pipe was completely covered. Note that stones must be placed carefully to avoid breaking the wave-pressure sensor probe on the pipe surface.

(2) Fill the test zone of the soil tank: The quartz sand and water are continuously stirred into a mixture and then gradually poured into the soil tank test section, stirring until a uniform liquid state is reached. When the sand is filled, it is left for more than three days for the gas to drain and the sand to consolidate. The final thickness of the consolidated soil layer is about 0.32 m. The surface soil is levelled with a scraper before the test.

(3) Fill the wave flume with water: Open the top water valve and cautiously fill the tank with fresh water at the slowest possible rate until the water depth reaches 0.45 m. Special attention should be paid to preserving the soil morphology and preventing visible erosion.

(4) Turn on the wave-maker and start the test: Under the condition of wave-making alone, turn on the wave-maker. When the direction of water flow is consistent with or opposite to the direction of wave-making, it is necessary to open the water flow generator first, and then open the oscilloscope for wave-making after the water flow reaches a stable state.

(5) Collect experimental data: To ensure the full development and attainment of equilibrium in the vibration response of the sandy seabed soil, the data collection period should be at least 180 s. Measurements including wave height, wave pressure, and pore water pressure are collected, with the sampling frequency set at 100 Hz.

(6) Turn off the wave-maker and end the test: For the scenario involving a single regular wave, you may proceed by shutting off the wave-maker and concluding the experiment. In instances of wave and current interaction, initially deactivate the wave generator, followed by the current generator. After turning off the wave generator (current) instrument, the tank should remain stationary for 10–20 min so that the water surface can become still. Repeat steps 2 to 7 to complete the experiment run under all conditions.

(7) In the next group of experiments, only steps (4)~(6) need to be repeated under the same circumstances. When switching to the next test group, it is necessary to repeat steps (1)~(6).

3. Results and Discussion

This study primarily investigates the hydrodynamic alterations surrounding a submarine pipeline and seabed pore pressure under the impact of regular waves with or without current. The experimental outcomes are contrasted with the protective efficacy of geotextiles and stone covers on the pipeline. In this experiment, the intersection point between the seabed surface and the pipeline centerline is designated as the coordinate origin, with the x-axis positive direction aligned with the wave propagation direction and the z-axis positive direction extending upwards from the seabed surface. In subsequent analyses, η denotes the wave profile and $|p_{\mathrm{w}}|$ signifies the maximum dynamic wave pressure. Additionally, the time–history variation curve of pore pressure (denoted as p_{s}) and the vertical depth variation in seabed pore pressure under regular wave–current action are considered, as well as the pore pressure variation patterns at different positions of the pipeline (front, bottom, and back). It should be mentioned that the pore pressure here refers to the excess pore pressure, which means it needs to be subtracted from the static pore pressure. Furthermore, to more intuitively observe the changes in pore pressure within the seabed, the relevant data were nondimensionalized. The equation $p_0 = \gamma_w \cdot h$ is the static pore pressure on the seabed surface, where γ_w is the specific weight of the water and h is the water depth. The impact of wave factors such as wave height (H), wave period (T), and wave velocity (U) on seabed pore pressure distribution around the pipeline are analyzed.

3.1. Hydrodynamic Properties Surrounding the Pipeline Under Wave and Current Influence

3.1.1. The Wave Profile Surrounding the Pipeline

In the experiment, the wave-height gauge WHG2123 was used to measure the wave surface change above the pipe with or without protection. Figure 6 shows the time-series change curve of the wave front at the top of the pipe with or without protection under the influence of regular waves (and currents). It can be seen from the figure that the fluctuation ranges depending on whether or not there is protection, under the regular wave condition monitored by WHG2123, are [−37.25,59.51] and [−43.47,65.57], respectively. The addition of forward flow significantly accelerates the wave propagation, and the fluctuation range at the top of the unprotected pipe is significantly reduced (the fluctuation range is [−43.73,56.76], which is 7.84% lower than that under the condition of no current), while the fluctuation range of the geotextile- and stone-covered pipe is increased by 5.18%. This is because the existence of geotextile and stone cover increases the height of the structure to a certain extent, resulting in an increase in the fluctuation range. When the wave flow is reversed, the current will inhibit the wave propagation, the wave period will decrease, and the fluctuation amplitude of the pipe with or without protection will increase significantly. The fluctuation amplitudes of the pipe with and without protection are [−55.07,95.63] and [−54.12,86.88], respectively. Compared with the no-current condition, the fluctuation amplitude increased by 35.81% and 29.30%, respectively. It can be seen from the experiment that the effect of the reverse current on the wave is significant and cannot be ignored.

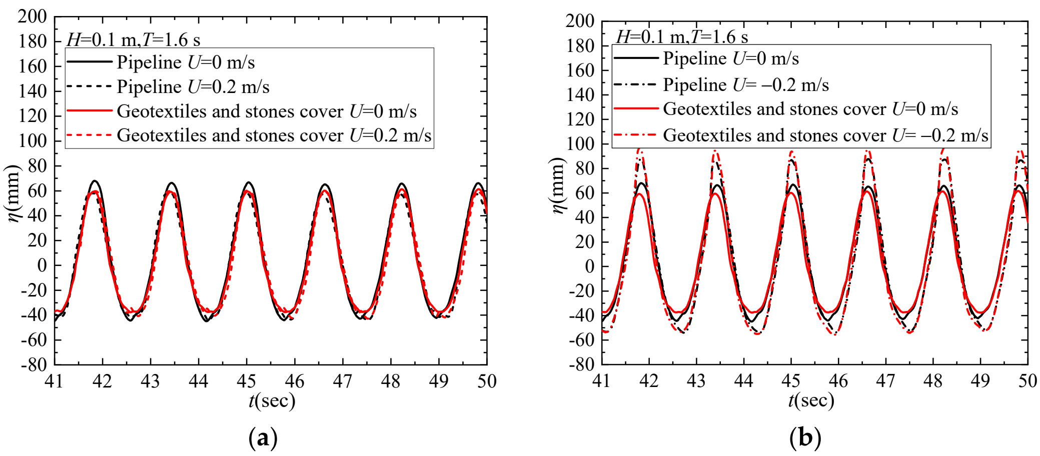

Figure 6. Wave profile above the pipe with and without geotextile and stone cover under wave action: (**a**) with forward current (U = 0.2 m/s); (**b**) with reverse current (U = −0.2 m/s). (H = 0.1 m; T = 1.6 s).

3.1.2. Dynamic Wave Pressures Around the Pipeline

Figure 7 illustrates the spatial distribution of dynamic wave pressure on the pipe surface, with and without geotextile and stone cover protection, under the influence of regular waves with varying wave characteristics. The maximum dynamic wave pressure is selected as the ordinate. When waves act alone, wave height is positively correlated with wave pressure, meaning that higher wave heights result in greater wave pressures. Due to the obstruction of wave energy propagation by the pipe, the maximum wave pressure at the pipe's bottom stagnation point is higher than at the top stagnation point, particularly at the 270° point on the pipe's surface. In comparison to the unprotected single pipe, the maximum wave pressure measured on the geotextile- and stone-protected pipe is reduced by 38.24%, and the distribution of wave pressure along the pipe's surface is more uniform, especially under the action of waves with higher wave heights. In the absence of protection, the wave pressure on the pipe surface is also positively correlated with the wave period. When the wave period reaches its maximum of T = 1.8 s, the wave pressure at 270° on the pipe surface reaches its peak. However, when the period is T = 1.8 s, the maximum dynamic wave pressure at 270° on the geotextile- and stone-covered pipe surface decreases, and the dynamic wave pressure at 270° on the geotextile- and stone-covered pipe surface is reduced by 41.56% under the action of a T = 1.8 s wave period.

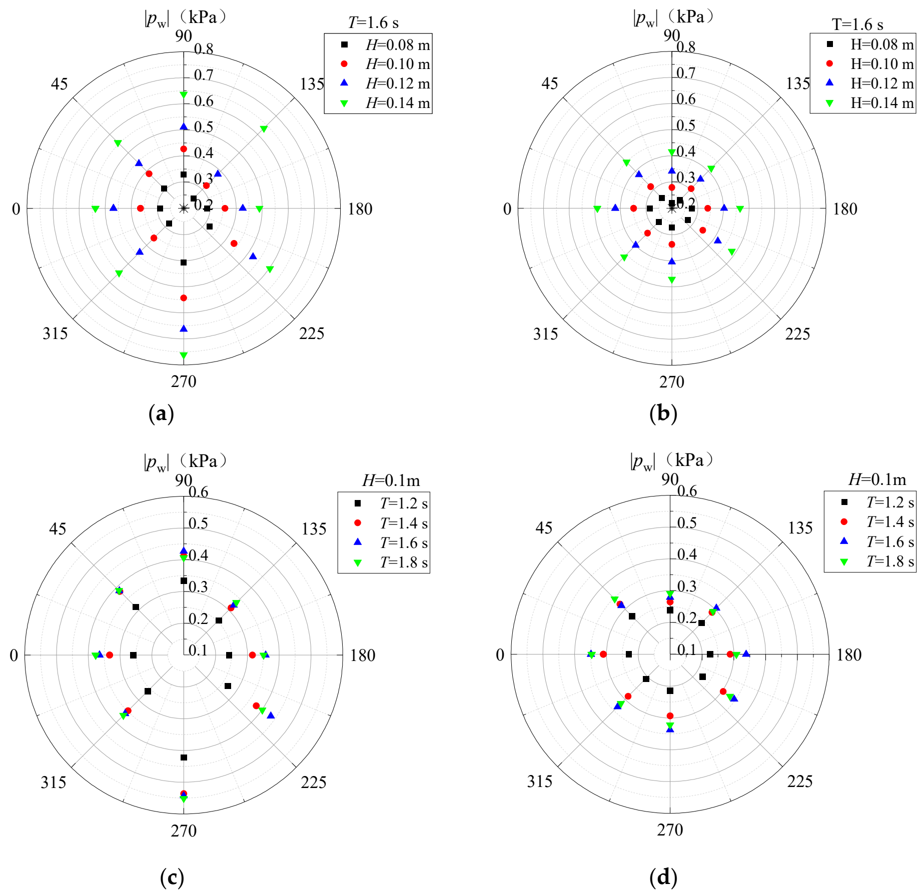

Figure 7. Maximum dynamic wave pressure around the pipe for different wave heights and periodic parameters under regular wave conditions: (**a**) without protection (T = 1.6 s); (**b**) with protection (T = 1.6 s); (**c**) without protection (H = 0.1 m); (**d**) with protection (H = 0.1 m).

Figure 8 illustrates the spatial distribution of dynamic wave pressure on the surface of the pipe with and without geotextile and stone protection under the combined action of regular waves and varying current rates (U). When the wave and current act in the same direction, taking the flow rate U = 0.2 m/s as an example, the maximum wave pressure value of the pipe under the protection of geotextiles and stones is reduced by 24.03% compared with that of the pipe without protection. When the wave and the flow act in the opposite direction, for example, U = −0.2 m/s, compared with the unprotected pipe, the maximum wave pressure value of the pipe under the protection of geotextiles and stones is reduced by 40.51%, and the protection effect on the bottom of the pipe is obvious. These comprehensive results show that the effect of geotextiles and stones acting as hydrodynamic protection around the pipe is remarkable, considering wave action with a large wave height and wave period, as well as wave–current action.

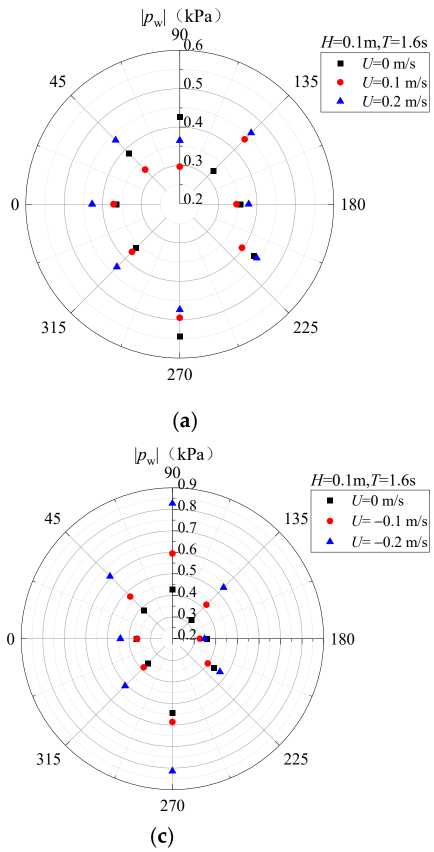

Figure 8. Maximum dynamic wave pressure around the pipe with different current velocity parameters under regular wave–current conditions: (**a**) without protection (H = 0.1 m, T = 1.6 s); (**b**) with protection (H = 0.1 m, T = 1.6 s); (**c**) without protection (H = 0.1 m, T = 1.6 s); (**d**) with protection (H = 0.1 m, T = 1.6 s).

3.2. Seabed Response Around the Pipeline Under Wave–Current Action

Figure 9 shows the time series of pore pressure induced by waves (and currents) beneath the bottom of the pipeline, resulting in either exposure to hydrodynamic actions or backfilling with geotextile and stone cover. The pore pressure in this paper is the excess pore pressure p_s after subtracting the hydrostatic pressure. Due to the energy dissipation caused by sediment particles, the pore pressure attenuates gradually in the seabed depth direction. The pore pressure amplitude at different layers of the geotextile- and stone-covered protected pipeline is much smaller than that of the unprotected pipeline. Meanwhile, it can be seen from the figure that the influence of the current direction on the pore pressure in the seabed is obvious. Compared with the reverse current, the maximum pore pressure amplitudes at p31, p32, p33, and p34 of the unprotected pipeline increase by 0.04 kPa, 0.05 kPa, 0.07 kPa, and 0.09 kPa, respectively, under the wave condition with forward current. The maximum pore pressure amplitudes at p31, p32, p33, and p34 of the geotextile- and stone-covered pipeline, on the other hand, are increased by 0.04 kPa, 0.05 kpa, 0.07 kPa, and 0.06 kPa, respectively. This demonstrates that the forward current can promote wave conduction along the seabed depth with regard to that under the reverse current condition; as a consequence, the pore pressure in the profile of seabed depth becomes larger when the current and the wave travel in the same direction. This is ascribed as the reason that the forward current enhances the permeability of wave energy into the seabed. Moreover, the protective effect of the geotextile and stone cover means that the current has little effect on the pore pressure on the seabed surface, particularly below z = −0.12 m (p33), which is also reflected in Section 3.4.3.

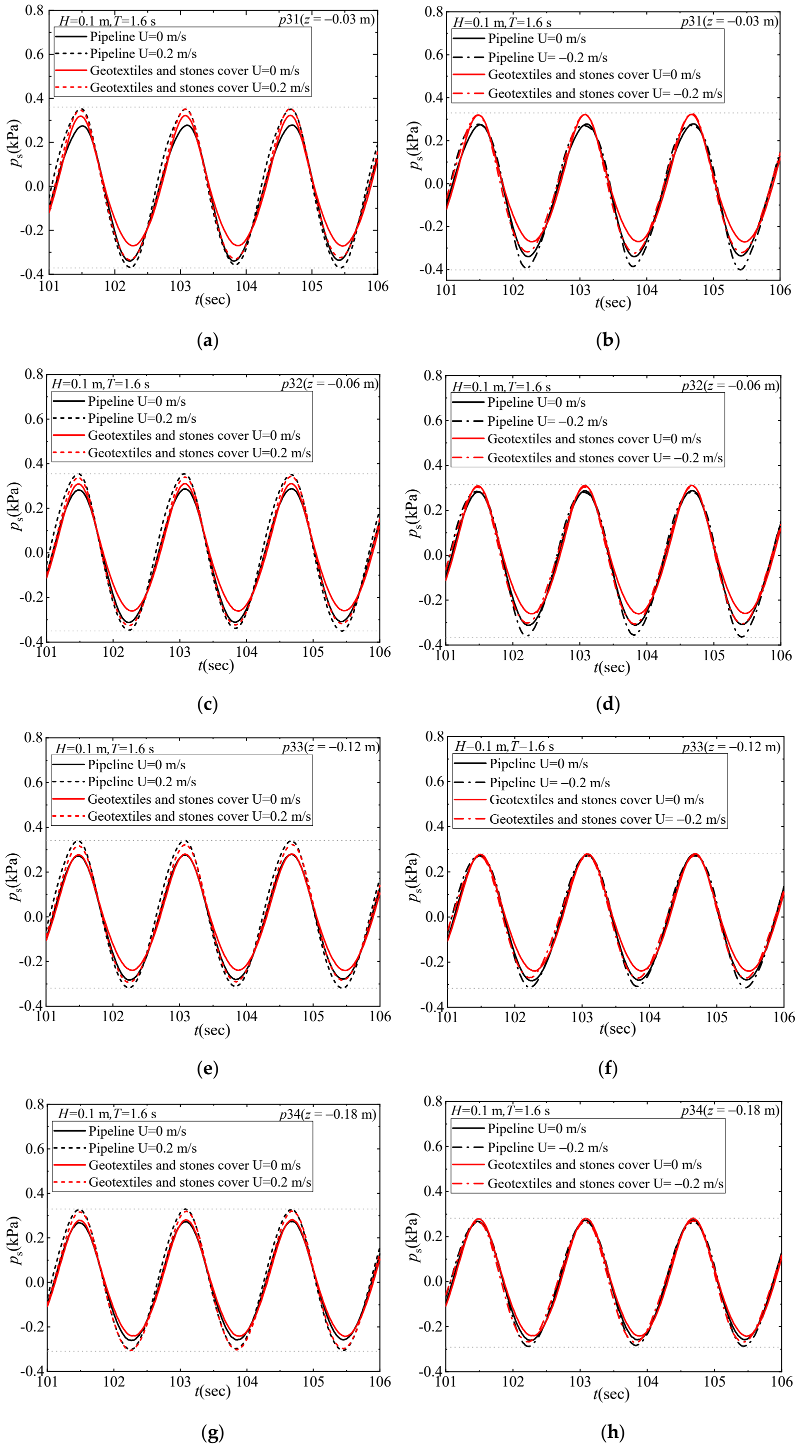

Figure 9. Time history of the pore pressures from −0.03 m to −0.18 m on the seabed surface of the bottom of the pipe with or without geotextile and stone cover protection under the action of waves with forward currents (U = 0.2 m/s) or reverse currents (U = −0.2 m/s): (**a**,**b**)—pore pressure at point p31; (**c**,**d**)—pore pressure at point p32; (**e**,**f**)—pore pressure at point p33; (**g**,**h**)—pore pressure at point p34. (H = 0.1 m; T = 1.6 s).

3.3. Influence of Protection Layer Properties on Seabed Response

Figure 10 shows the distribution and variation patterns of excess pore pressure within the seabed at different positions around the pipelines with and without the protection of geotextiles and stone cover, with four layers of pore pressure sensors arranged at four depth directions of z = −0.03 m, −0.06 m, −0.12 m, and −0.18 m. $|p_s|/p_0$ represents the dimensionless maximum excess pore pressure caused by waves (current). Considering the wave-alone situation, as seen in Figure 10a, the pore pressure underneath the unprotected pipeline is obviously smaller than the pore pressure at the far end of the seabed. The attenuation of wave energy along the propagation approach caused by the porosity property of the seabed contributes to this phenomenon. Furthermore, as the depth of the seabed near the pipeline increases, the rate of pore pressure dissipation gradually slows down, indicating that the pipeline has a certain protective effect on the surrounding area. Comparing Figure 10a,b, the pore pressure around the geotextile- and stone-covered protected pipeline does not change obviously in comparison to that in the vicinity of the exposed pipeline, and the pore pressure amplitudes of the front, bottom, and back of the pipelines are roughly the same.

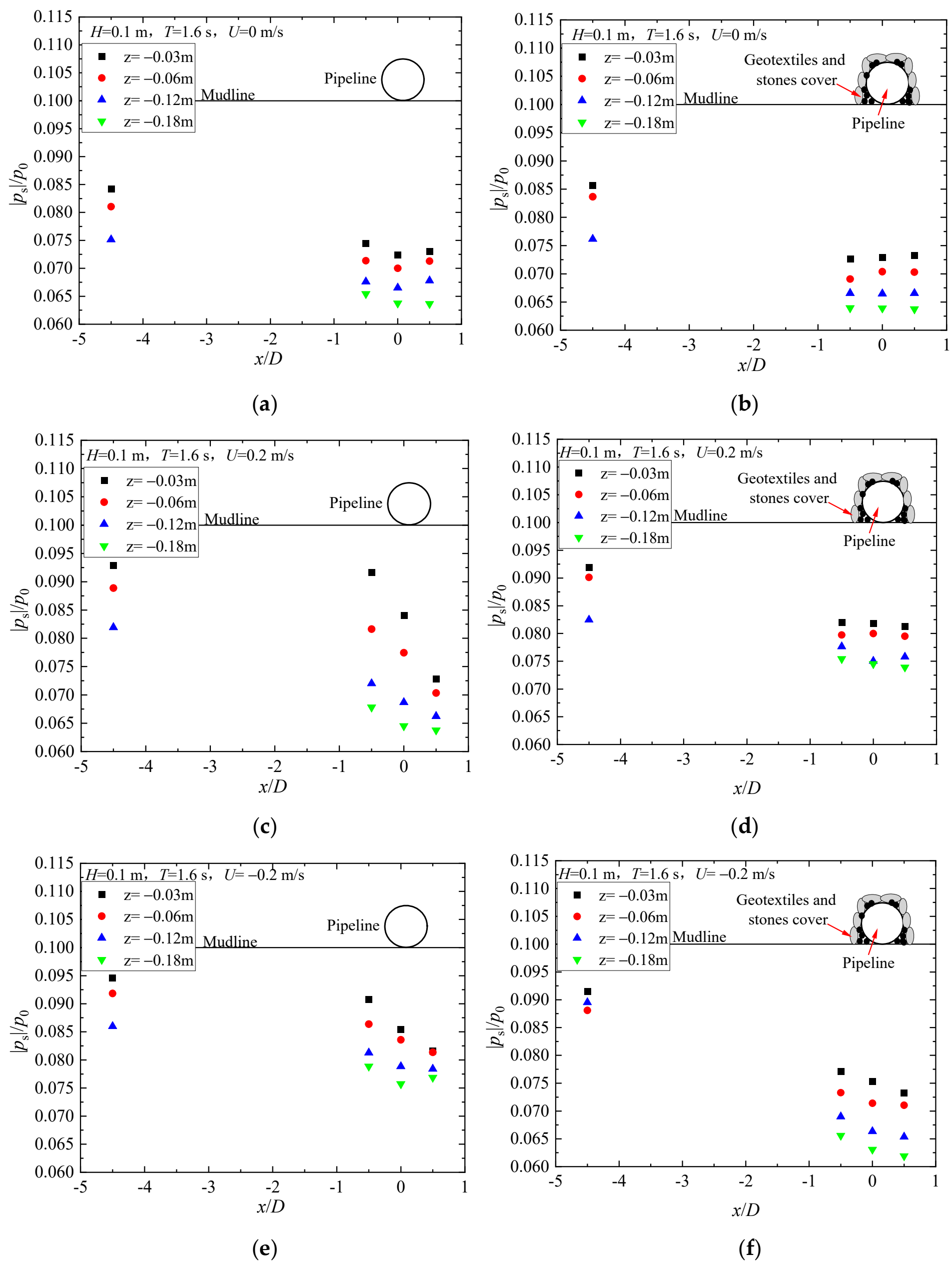

Figure 10. Variation in the measured pore pressure amplitude at different positions of the pipe with or without geotextile and stone cover protection: (**a**) without protection (U = 0 m/s); (**b**) with protection (U = 0 m/s); (**c**) without protection (U = 0.2 m/s); (**d**) with protection (U = 0.2 m/s); (**e**) without protection (U = −0.2 m/s); (**f**) with protection (U = −0.2 m/s). (H = 0.1 m; T = 1.6 s).

When the wave superimposes a forward current, as seen in Figure 10c,d, the change in velocity has a significant effect on the amplitude of the pore pressure around the fully exposed pipeline, and the influence degree of current on the pore pressure amplitude decreases with the depth of the seabed. This is mainly due to the obstructing effect of the pipeline on the fluid field, which reduces the wave pressure exerted on the seabed surface behind the pipe, thus weakening the infiltration effect of current flow on the pore pressure on the seabed. However, the protection layer of the geotextile and stones embedded on the pipeline blocks the current propagation, leading to the pore pressure amplitude not changing significantly. As seen in Figure 10e,f, when waves are superimposed by a reverse current, the impact of velocity change on the amplitude of pore pressure around the unprotected pipeline is smaller than that under the condition of the wave and current in the same direction. However, the amplitude of the pore pressure in front, at the bottom, and at the back of the protected pipeline is much smaller than that within the seabed around the unprotected pipeline. That is, the sheltering function of the geotextile and stone coverage serves as the pipe's protection measure; this is obvious when the current travels against the wave.

3.4. Influence of Wave and Current Parameters on Seabed Response

3.4.1. Impact of Wave Height Parameters

The influence of waves with diverse wave heights on the seabed pore pressure around the unprotected pipe is discussed. The fixed period T = 1.6 s. Figure 11 shows the vertical distribution of excess pore pressure in the seabed around the bottom of the pipes with and without protection versus various wave heights (z/h represents the dimensionless vertical depth of the seabed). With the increase in soil depth, pore pressure gradually dissipates. The effect of wave height on the pore pressure at the bottom of the unprotected pipe is concentrated in the upper seabed $z/h = -0.09$, and the effect of geotextile and stone load on the pore pressure at the bottom of the protected pipe is concentrated in the upper seabed $z/h = -0.38$. Due to the positive correlation between wave energy and wave height, the pore pressure amplitudes of the seabed in both cases (with and without geotextile- and stone-covered protective pipe) increase with the increase in wave height and reach the maximum value when H = 0.14 m. With regard to the pore pressure of w7($z/h = 0$) near the seabed surface, as the wave height increases from 0.08 m to 0.14 m at an interval of 0.02 m, the percentage increases in pore pressure measured under the unprotected pipe are 33.70%, 21.95%, and 14.67%, respectively, while the percentage increases in pore water pressure measured for the geotextile- and stone-covered pipe are 22.58%, 21.05%, and 14.13%, respectively. Thus, the effect of wave height on pore pressure amplitude decreases with the increase in wave height. Moreover, compared with the unprotected pipe, the pore pressure measured for the protected pipe (w7) decreased by 32.61%, 38.21%, 38.67%, and 38.95%, respectively, when the wave height increased. The effect of geotextile and stone protection on wave height and pore pressure amplitude increases with the increase in wave height. That is, the greater the wave height, the better the wave protection effect.

3.4.2. Impact of Wave Period Parameters

The responses of the seabed around the pipelines to waves with diverse wave periods are discussed. The fixed wave height H = 0.1 m. Figure 12 shows the vertical distribution of excess pore pressure in the seabed around the bottom of the pipes with and without protection at various wave periods. The results show that, under wave load, the pore pressure amplitude at the bottom of the pipe without protection increases with the increase in the wave period. Meanwhile, the attenuation rate of pore pressure versus the depth of the seabed becomes slower with the increase in the wave period. When the period increases from 1.2 s to 1.8 s at an interval of 0.2 s, the increases in pore pressure around the unprotected pipe are 26.04%, 2.48%, and 1.61%, respectively, whereas the increment percentages of pore water pressure measured for the geotextile- and stone-protected pipeline are 37.50%, 15.15%, and 0, respectively. The effect of wave period on pore pressure amplitude also decreases with the increase in wave period, and the effect of wave period on pore pressure amplitude is much smaller than that of wave height on pore pressure. Similarly, the wave protection effect of the geotextile and stones on the pipe is more significant with a greater wave period.

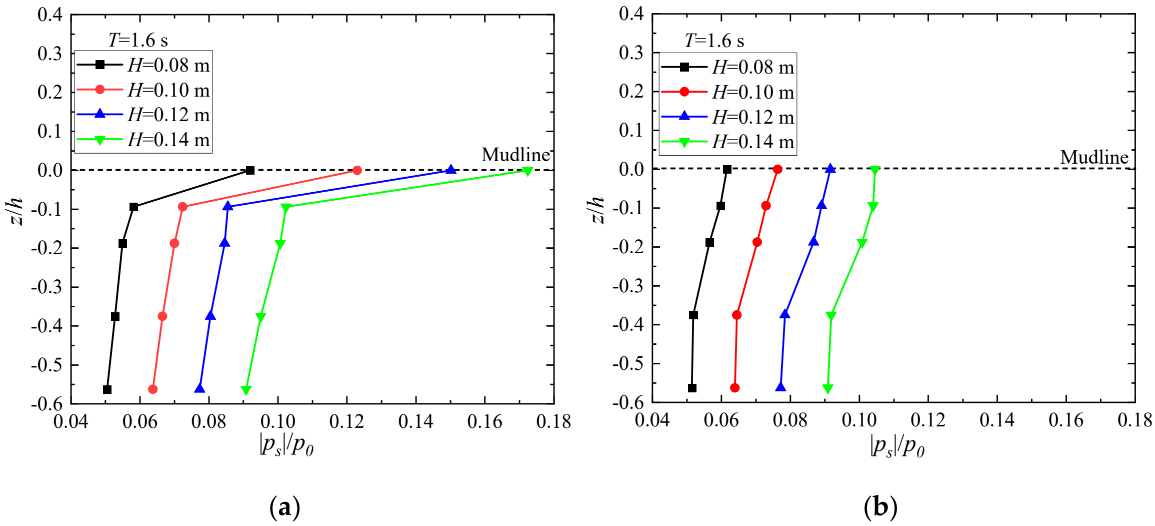

Figure 11. Vertical distributions of the maximum pore pressure ($|p_s|/p_0$) caused by waves at the bottom of the pipes (w7, p31, p32, p33, p34) with and without geotextile and stone protection, distributed vertically along the seabed depth (z/h). For different wave heights: (**a**) without protection; (**b**) with protection. (T = 1.6 s).

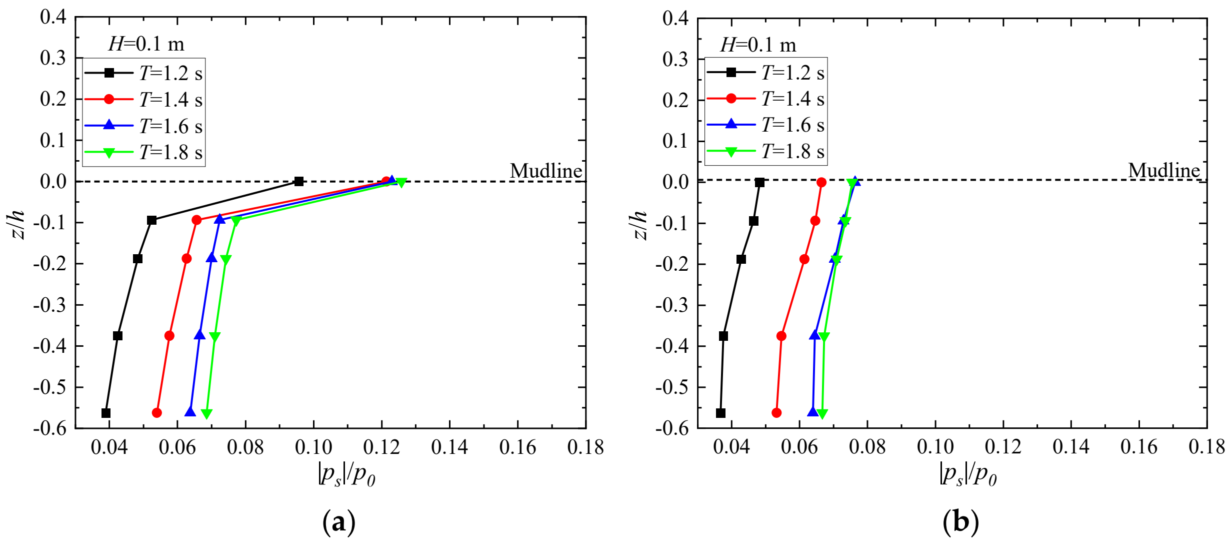

Figure 12. Vertical distributions of the maximum pore pressure ($|p_s|/p_0$) caused by waves at the bottom of the pipes (w7, p31, p32, p33, p34) with and without geotextile and stone cover protection, distributed vertically along the seabed depth (z/h). For different wave periods: (**a**) without protection; (**b**) with protection. (H = 0.1 m).

3.4.3. Impact of Current Parameters

We further analyzed the effect of the superposed regular wave with different current rates on the seabed pore pressure around the unprotected pipe (note that the forward flow is positive, the reverse flow is negative, and the symbol only represents the direction, not the size). The fixed wave height H = 0.1 m and the period T = 1.6 s. Figure 13 shows the vertical distribution of excess pore pressure at the bottom of the unprotected pipe at different current rates. The presence of water flow will affect the wave action and make the decay rate of pore pressure in the vertical direction change irregularly, especially in the countercurrent action.

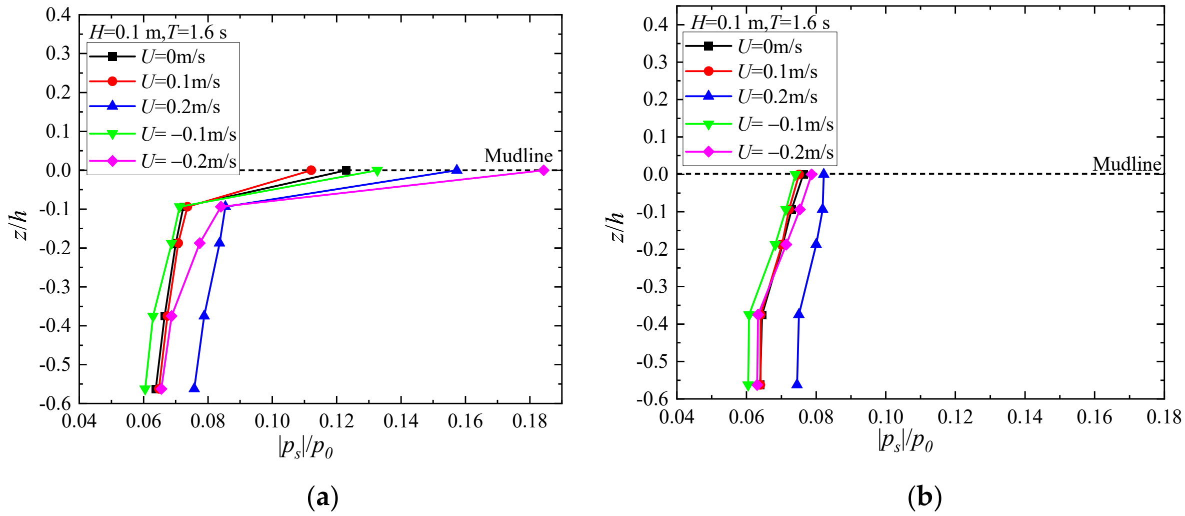

Figure 13. Vertical distributions of the maximum pore pressure ($|p_s|/p_0$) caused by waves at the bottom of the pipes (w7, p31, p32, p33, p34) with and without geotextile and stone cover protection, distributed vertically along the seabed depth (z/h). For different current velocities: (**a**) without protection; (**b**) with protection. (H = 0.1 m; T = 1.6 s).

When the wave–current action increases from U = 0 m/s to U = 0.2 m/s, the pore pressure amplitude at the bottom of the pipe increases by 27.64% and 7.89% in the case of the unprotected and geotextile- and stone-protected pipes, respectively. However, when the reverse action of wave–current increases from U = 0 m/s to U = −0.2 m/s, the measured pore pressure amplitude of the pipe bottom increases by 49.59% and 2.63% in the case of the unprotected and geotextile- and stone-protected pipes, respectively. When the current rates are U = 0 m/s, U = 0.2 m/s, and U = −0.2 m/s, the pore pressure amplitude measured for the geotextile- and stone-protected pipe decreases by 38.21%, 47.77%, and 57.60%, respectively, compared with that measured for the unprotected pipe. Therefore, this shows that geotextile and stone cover protection still has a significant protective effect on the pipe under the combined action of wave and current load, and the applicability to the sea condition of wave and reversed current is the most obvious, making this approach the best choice for pipe protection measures.

4. Conclusions

In this paper, wave–current flume experiments were conducted to study the dynamic wave pressure and pore pressure around submarine pipelines with and without geotextile and stone cover under the influence of regular waves and regular wave–current combined action. The protective effects of geotextiles and stones were compared and analyzed. Based on the summary analysis of the experimental results, the following conclusions can be drawn:

(1) Compared with the unprotected pipeline, the dynamic wave pressure on the surface of the protected pipeline decreases when the wave and current are superimposed. The change is smaller when the wave height and the wave period become larger, which indicates that the protection effect of geotextiles and stones covering the pipeline is more significant when the wave height and wave period are larger and the water and current are superimposed.

(2) The pore pressure driven by wave (and current) load decreases continuously with the seabed depth profile, and the pore pressure amplitude in the seabed around the geotextile- and stone-covered pipeline is smaller than that around the unprotected pipeline. In addition, the protective effect of the geotextile and stone covering layer makes the effect of current on pore pressures below $z = -0.12$ m on the seabed surface small. Compared with the single wave load, the forward current can promote the wave propagation speed; the velocity of wave propagation is inhibited by the reverse current. As a result, the common current promotes pore pressure conduction through the depth of the seabed, enhancing the greater permeability of waves into the seabed compared to the opposite current. That is, when waves act in the same direction as ocean currents, pipelines are more vulnerable to potential instability on the seabed.
(3) Under the combined action of waves and current, the pore pressure amplitudes of the front, bottom, and back of the geotextile- and stone-covered protected pipeline are basically the same, and the pore pressure is much smaller than that of the unprotected pipeline. However, the amplitude of the pore pressure around the unprotected pipe varies greatly, especially when the wave current is acting in the same direction.
(4) The pore pressure amplitude increases with the increase in wave height and period. The presence of current will affect the wave profile and make the attenuation rate of vertical pore pressure change irregularly. The effect of the geotextile and stone covering reduces the pore pressure around the pipeline, and the protective effect is more obvious when the current superposition wave is larger and the wave period is longer.

In this study, the wave tests only consider the protective effect of geotextiles and stones covering a submarine pipeline under the action of regular waves and regular wave–current action. However, in a real marine environment, the effects of random waves and random current characteristics cannot be ignored. Therefore, it is necessary to further study the protection effect of geotextiles and stones covering a submarine pipeline under random wave–current conditions. In terms of submarine pipeline protection, it is necessary to increase the research on other pipeline protection measures, such as covering the pipeline surface with protective pads or rigid protective covers. In addition, this experiment only compares and measures wave-induced pore pressure around protected and unprotected pipelines, but the relationship between local erosion and pore pressure around geotextile- and stone-covered pipelines is not available in the literature. In addition, this paper only focuses on physical modeling and does not carry out numerical simulation. The effect of the geotextile- and stone-covered pipeline on seabed response and liquefaction potential under different seabed parameters, as well as regular spectra and random spectra, can be further studied by numerical simulation in the future.

Author Contributions: Conceptualization, K.S., B.C. and D.-S.J.; methodology, D.-S.J., L.C. and R.W.; investigation, W.S., M.W. and Y.G.; resources, D.-S.J., K.S., B.C., L.C., R.W. and H.Z.; data curation, W.S., M.W. and Y.G.; writing—original draft preparation, W.S.; writing—review and editing, K.S., B.C., D.-S.J., L.C. and H.Z.; visualization, W.S.; supervision, K.S., B.C. and R.W.; project administration, K.S.; funding acquisition, K.S. All authors have read and agreed to the published version of the manuscript.

Funding: This research was jointly supported by the Doctoral Research Foundation Project of Shandong Jiaotong University (BS2021006), the National Natural Science Foundation of China (Grant No: 52271281), and the Shandong Provincial High-Level Talent Workstation.

Institutional Review Board Statement: Not applicable.

Informed Consent Statement: Not applicable.

Data Availability Statement: The experimental data are available upon request to the corresponding author.

Conflicts of Interest: The authors declare no conflicts of interest.

References

1. Herbich, J.B. *Offshore Pipe Design Elements*; Marcel Dekker Inc.: New York, NY, USA, 1981.
2. Demars, K.R.; Vanover, E.A. Measurement of wave-induced pressures and stresses in a sand bed. *Mar. Georesour. Geotechnol.* **1985**, *6*, 29–59. [CrossRef]
3. Jas, E.; O'Brien, D.; Fricke, R.; Gillen, A.; Cheng, L.; White, D.; Palmer, A. Pipeline stability revisited. *J. Pipeline Eng.* **2012**, *11*, 259–268.
4. De, R.J.; De, M.C. Port structures, their care and maintenance. *Bull. Perm. Int. Assoc. Navig. Congr.* **1987**, *58*, 133–168.
5. Silvester, R.; Hsu, J.R.C. Sines revisited. *J. Waterw. Port Coast. Ocean Eng.* **1989**, *115*, 327–343. [CrossRef]
6. Kramer, S.L. Triggering of liquefaction flow slides in coastal soil deposits. *Eng. Geol.* **1988**, *26*, 17–31. [CrossRef]
7. Kramer, S.L.; Seed, H.B. Initiation of soil liquefaction under static loading conditions. *J. Geotech. Eng.* **1988**, *114*, 412–430. [CrossRef]
8. Liu, Y.; Hu, H.; Zhang, D. Probability analysis of damage to offshore pipeline by ship factors. *Transp. Res. Rec.* **2013**, *2326*, 24–31. [CrossRef]
9. Muhlbauer, W.K. *Pipeline Risk Management Manual: Ideas, Techniques, and Resources*; Gulf Professional Publishing: Houston, TX, USA, 2004.
10. Sudhan, C.M.; Sundar, V.; Rao, S.N. Wave induced forces around buried pipelines. *Ocean Eng.* **2002**, *29*, 533–544. [CrossRef]
11. Zhou, C.; Li, G.; Dong, P.; Shi, J.; Xu, J. An experimental study of seabed responses around a marine pipeline under wave and current conditions. *Ocean Eng.* **2011**, *38*, 226–234. [CrossRef]
12. Chen, H.; Zhang, J.; Tong, L.; Sun, K.; Guo, Y.; Wei, C. Experimental study of soil responses around a pipe in a sandy seabed under wave-current load. *Appl. Ocean Res.* **2023**, *130*, 103409. [CrossRef]
13. Zhai, Y.; He, R.; Zhao, J.; Zhang, J.; Jeng, D.S.; Li, L. Physical model of wave-induced seabed response around trenched pipeline in sandy seabed. *Appl. Ocean Res.* **2018**, *75*, 37–52. [CrossRef]
14. Sun, K.; Zhang, J.; Gao, Y.; Jeng, D.S.; Guo, Y.; Liang, Z. Laboratory experimental study of ocean waves propagating over a partially buried pipeline in a trench layer. *Ocean Eng.* **2019**, *173*, 617–627. [CrossRef]
15. Gao, Y.; Lin, J.; Zhang, J.; Guo, Y. Numerical modeling of combined wave and current-induced residual liquefaction around twin pipelines. *Ocean Eng.* **2022**, *261*, 112134. [CrossRef]
16. Sumer, B.M.; Fredsøe, J. *The Mechanics of Scour in the Marine Environment*; World Scientific Publishing Company: Singapore, 2002.
17. Sekiguchi, H.; Sassa, S.; Miyamoto, J.; Sugioka, K. Wave-induced liquefaction, flow deformation and particle transport in sand beds. In Proceedings of the ISRM International Symposium, Melbourne, Australia, 19–24 November 2000.
18. Sumer, B.M.; Dixen, F.H.; Fredsøe, J. Cover stones on liquefiable soil bed under waves. *Coast. Eng.* **2010**, *57*, 864–873. [CrossRef]
19. Sumer, B.M.; Dixen, F.H.; Fredsøe, J. Stability of submerged rock berms exposed to motion of liquefied soil in waves. *Ocean Eng.* **2011**, *38*, 849–859. [CrossRef]
20. Tauqeer, M.A. Geometry Optimization of Glass Reinforced Plastic (GRP) Subsea Protection Covers. Master's Thesis, University of Stavanger, Stavanger, Norway, 2016.
21. Yin, G.; Gorikhin, A.; Olsen, C.L.; Liu, S.; Ong, M.C. Numerical simulations of wave-soil-structure interactions for a subsea cover. *Coast. Eng.* **2024**, *189*, 104475. [CrossRef]
22. Ates, B.; Sadoglu, E. A quasi-2D exploration of optimum design settings for geotextile-reinforced sand in assistance with PIV analysis of failure mechanism. *Geotext. Geomembr.* **2023**, *51*, 418–436. [CrossRef]
23. Ateş, B.; Şadoğlu, E. Experimental Investigation for Failure Mechanism and Bearing Capacity of Strip Footing on Soil Reinforced with Geotextile Following the Shukla's Wraparound Reinforcement Technique. *Int. J. Geosynth. Ground Eng.* **2024**, *10*, 5. [CrossRef]
24. Wang, J.Q.; Zhang, L.L.; Xue, J.F.; Tang, Y. Load-settlement response of shallow square footings on geogrid-reinforced sand under cyclic loading. *Geotext. Geomembr.* **2018**, *46*, 586–596. [CrossRef]
25. Xie, L.; Zhu, Y. Scour protection of underwater pipelines. *J. Civil Eng. Constr.* **2018**, *7*, 171–177. [CrossRef]
26. Zhang, B.; Gong, R.; Wang, T.; Wang, Z. Causes and treatment measures of submarine pipeline free-spanning. *J. Mar. Sci. Eng.* **2020**, *8*, 329. [CrossRef]
27. Gao, F.P.; Gu, X.Y.; Jeng, D.S. Physical modeling of untrenched submarine pipeline instability. *Ocean Eng.* **2003**, *30*, 1283–1304. [CrossRef]
28. Wang, M.; Si, W.; Gao, Y.; Cui, L.; Jeng, D.S.; Sun, K.; Chen, B.; Zhao, H. Experimental Study of the Random Wave-Induced Hydrodynamics and Soil Response in a Porous Seabed Around Double Piles. *J. Mar. Sci. Eng.* **2024**, *12*, 1715. [CrossRef]
29. Xu, Y.; Cui, L.; Jeng, D.S.; Sun, K.; Chen, B. Laboratory Investigations on Oscillatory Seabed Responses and Scour Around a Pipeline Under Wave-Current Loading. In Proceedings of the ASME 2024 43rd International Conference on Ocean, Offshore and Arctic Engineering, Singapore, 9–14 June 2024.